Check for updates

ADVANCED MATERIALS TECHNOLOGIES
www.advmattechnol.de

Magnetic Nozzle-Free Embedded 3D (MagNoFE3D) Printing

Franco N. Piñan Basualdo, Vasileios D. Trikalitis, Sabrina Visconti, Fanny Ficuciello, Constantinos Goulas, Jeroen Rouwkema, and Sarthak Misra*

The functional principle behind extrusion-based printing is the capability of flowing material through a nozzle on demand, which must solidify upon deposition, a behavior exhibited only by some materials. Embedded printing offers a solution to maintain shape fidelity during the deposition of a wider range of materials. However, the use of a moving nozzle in a support bath can lead to bath disturbance and the spreading of the ink. In this study, a novel embedded printing technique that eliminates the need for a nozzle by employing a magnetic sphere as the plotting moiety is introduced. The externally steered sphere creates a path by locally fluidizing the bath, allowing the simultaneously injected ink to flow into the space behind it. The method is benchmarked using water as an ink, achieving free-form printing without additional stabilization methods. The creation of solid structures is also demonstrated by printing a photocurable ink that is crosslinked and removed from the bath. Moreover, the plotting magnet can be incorporated into the printed part during the crosslinking, thus giving place to a magnetically responsive structure. This advancement paves the way for innovations in fields such as tissue engineering and microrobotics by enabling the fabrication of intricate and functional designs.

1. Introduction

One of the most popular 3D printing approaches is extrusion-based printing,[1] which is employed in a plethora of fields such as tissue engineering,[2] soft robotics,[3] and drug tablet 3D printing.[4] Extrusion printing consists of extruding through a moving nozzle an ink material that exhibits low viscosity under shear stress but quickly rigidifies upon deposition, a behavior known as thixotropic,[5] to retain its shape.[6] This principle significantly limits the range of materials that can be printed without further processing since thixotropic is only exhibited by gels, colloids, and other complex materials.[7] To imitate this rheological behavior, some alternatives exist to print non-thixotropic materials, such as melting the material to extrude it and cooling post-deposition to solidify, known as Fused Deposition Modeling,[8] in-line or post-deposition photopolymerization,[9] in situ crosslinking[10] or using sacrificial support structures.[11] In particular, PolyJet printing, which jets photopolymer onto the build platform and rapidly cures it with ultraviolet (UV) lamps, has emerged as a standard for precise multi-material 3D printing of photocurable low-viscosity inks.[12] However, these techniques are often incompatible with bioprinting applications, as biological materials cannot withstand the rapid temperature changes or intense UV irradiation required during the process. In this context, a paradigm shift was triggered through embedded printing[13] which utilizes support baths to print materials that are not able to retain their shape post-deposition in extrusion printing.

F. N. Piñan Basualdo, S. Visconti, S. Misra
Surgical Robotics Laboratory
Department of Biomechanical Engineering
University of Twente
Enschede 7522 NB, The Netherlands
E-mail: franconicolas.pinanbasualdo@kuleuven.be

V. D. Trikalitis, J. Rouwkema
Vascularization Laboratory
Department of Biomechanical Engineering
University of Twente
Enschede 7522 NB, The Netherlands

S. Visconti, F. Ficuciello
ICAROS and PRISMA Laboratories
Department of Electrical Engineering and Information Technology
University of Naples Federico II
Naples 80131, Italy

C. Goulas
Department of Design Production and Management and Technical Medical Centre
University of Twente
Enschede 7522NB, The Netherlands

S. Misra
Surgical Robotics Laboratory
Department of Biomaterials and Biomedical Technology
University of Groningen and University Medical Centre Groningen
Groningen 9713 GZ, The Netherlands

The ORCID identification number(s) for the author(s) of this article can be found under https://doi.org/10.1002/admt.202401097

© 2024 The Author(s). Advanced Materials Technologies published by Wiley-VCH GmbH. This is an open access article under the terms of the Creative Commons Attribution License, which permits use, distribution and reproduction in any medium, provided the original work is properly cited.

DOI: 10.1002/admt.202401097

Embedded printing consists of injecting ink through a moving nozzle in a support bath, which can be classified as either granular suspensions[14] or continuous viscoelastic matrices,[15] which stabilize the printed shape. Embedded printing has enabled the printing materials that were not able to retain their shape post-deposition such as low viscosity inks and Newtonian fluid suspensions of cells, particles, and spheroids.[16–20] Because of their biocompatibility, availability, and transparency, hydrogels, Carbomers, or hydrogel microparticles have been used as support baths.[14,20,21] Optimized ink-bath combinations have been used to print soft robots,[22] motion sensors,[23] and tissue[24] utilizing embedded printing. In embedded printing, the bath composition, printing speed, nozzle size and shape, and the interfacial tension between the ink and the bath are all parameters that determine the success or failure of the approach. For example, a deposited ink filament can break into droplets if the surface tension between the ink and the bath is too high due to the Rayleigh–Plateau instability.[25] On the other hand, the deposition of low-viscosity inks (<100mPas) can be challenging since the ink can spread upwards behind the moving nozzle, which depends on the nozzle diameter and viscosity ratio between the ink and the bath.[26] Two main strategies have been adopted to enable the printing of low-viscosity inks: chemical and fluidic stabilization. Chemical stabilization of the structure can be achieved, for example, by two-phase stabilization, in which the formation of a membrane between ink and bath stabilizes the structure,[27] or the use of core-shell nozzles, where the outer phase stabilizes the printed pattern.[28] On the other hand, fluidic stabilization aims at minimizing the spreading of the ink by optimizing the size or shape of the moving nozzle. The printing of aqueous viscosity inks (0.7 to 1.09mPa s) without a stabilizing media or chemical reactions are shown either with a custom glass capillary nozzle,[18] or a 90° bent nozzle.[20] Although embedded printing has been evolving rapidly, enabling the creation of increasingly complex structures, it faces a fundamental limitation when using a moving nozzle. Specifically, it is impossible to print a continuous and arbitrarily complex structure, such as a knot, because the nozzle movement would inevitably disrupt already printed sections.

One alternative to prevent the disruption of already printed sections is the exploitation of magnetic actuation. Magnetic actuation offers the possibility to remotely manipulate objects by adjusting the currents circulating through a set of coils surrounding the workspace.[29] Additionally, the recent development of closed-loop control algorithms enables the precise control of one[30,31] or multiple[32,33] objects in a 3D space. Magnetically actuated microrobots can perform tasks in confined environments, making them ideal for applications in targeted drug delivery, minimally invasive surgery, and micro-assembly.[34,35] The integration of magnetic actuation into embedded 3D printing can enable the remote manipulation of the printing process, thus preventing the disturbance of already printed sections.

In this work, we develop an embedded printing methodology that eliminates the need for a nozzle, instead using a magnetic sphere as the plotting moiety, termed the Magnetic Nozzle-Free Embedded 3D (MagNoFE3D) technique. To demonstrate that this methodology is suitable for printing low-viscosity inks, we benchmarked the capabilities of our proposed methodology by printing straight and 3D shapes with water. This confirmed that true free-form printing of water is achievable with our approach, without the need for additional stabilization methods. Additionally, we demonstrated the compatibility of our technique with photopolymerization printing of solid structures by using a photocurable ink to plot a pattern, crosslink it, and subsequently remove the support bath. The ability to incorporate magnets into polymeric structures for remote actuation has been demonstrated in prior research, especially in developing magneto-sensitive materials for soft robotics and microrobotics applications.[36] However, these approaches typically involve embedding magnets after the printing process[37] or using a suspension of magnetic particles as ink,[38] which may introduce limitations in terms of the precision or material of the printed structures. By contrast, MagNoFE3D enables the incorporation of the magnetic sphere directly during the printing process by leaving the magnet in the bath during photopolymerization, eliminating the need for additional embedding steps.

2. Results and Discussion

2.1. Proposed System

Our Magnetic Nozzle-Free Embedded 3D (MagNoFE3D) printing replaces the moving nozzle of traditional embedded printing with an externally controlled magnet which opens a path in the support bath to guide the ink, as shown in **Figure 1**. As a support bath, we use a Carbopol gel suspension, a granular material with yield-stress characteristics that behaves as an elastic solid under low shear stress (unyielded) and transitions to a non-Newtonian fluid at higher shear stress (yielded). By remotely exerting magnetic forces, the magnet can be steered in the support bath to follow arbitrary 3D trajectories. The movement of the magnet locally fluidizes the support bath, opening space for the ink that is simultaneously injected. Since the rest of the bath remains unyielded, the ink will fill the space behind the magnet, following the path of least resistance. The main advantage of this approach is that, unlike in the moving nozzle approach, the support bath is only locally fluidized, preventing the disruption of already printed sections.

The proposed MagNoFE3D printing system consists of a syringe pump for injecting the ink and an electromagnetic actuation system[33] for steering the magnet, as shown in Figure 1A,B. The electromagnetic actuation system consists of nine electromagnetic coils surrounding the workspace to generate the required 3D magnetic field and gradient. Two orthogonal cameras (side and top views) complete the actuation system to track the magnet in real-time and adjust the exerted magnetic force accordingly. The actuation system is directed by a computer and custom-made control software. To validate the proposed approach, the magnet-fluid dynamics are analyzed in the next section.

2.2. Magnet-Fluid Dynamics

The dynamics of a magnet in a fluid bath are governed by a combination of the magnetic effects and the support bath density and

© 2024 The Author(s). Advanced Materials Technologies published by Wiley-VCH GmbH

2365709x, 0, Downloaded from https://onlinelibrary.wiley.com/doi/10.1002/admt.202401097 by Universiteitsbibliotheek, Wiley Online Library on [11/10/2024]. See the Terms and Conditions (https://onlinelibrary.wiley.com/terms-and-conditions) on Wiley Online Library for rules of use; OA articles are governed by the applicable Creative Commons License

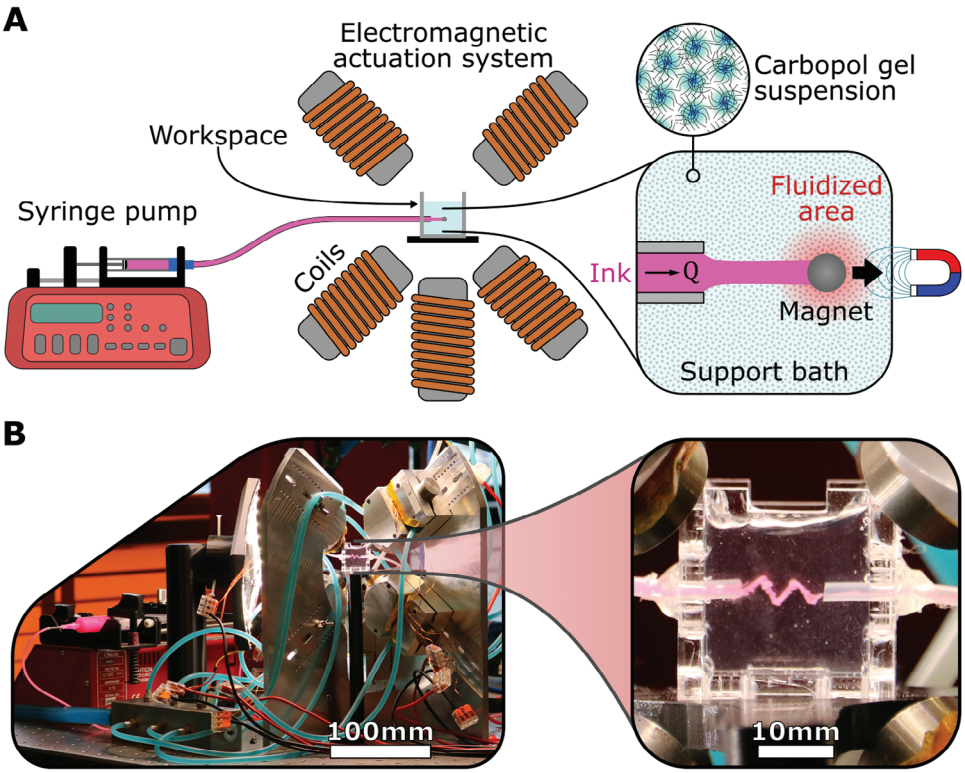

Figure 1. Magnetic Nozzle-Free Embedded 3D (MagNoFE3D) printing concept. A) MagNoFE3D embedded printing system consisting of an injecting syringe pump (injection flow (Q)) and an electromagnetic system to steer the plotting magnet. The movement of the magnet locally fluidizes the yield-stress support bath, opening space and guiding the ink. In this case, the utilized support bath is a granular Carbopol gel suspension. B) Picture of the experimental setup and a double helix printed with colored water.

rheological properties. A magnet in a magnetic field ($\mathbf{B}$) experiences a magnetic torque ($\mathbf{T}_{mag}$) and force ($\mathbf{F}_{mag}$) as

$$\begin{aligned} \mathbf{T}_{mag} &= \mathbf{m} \times \mathbf{B} \\ \mathbf{F}_{mag} &= (\mathbf{m} \cdot \nabla)\mathbf{B} \end{aligned} \tag{1}$$

where $\mathbf{m} = V\mathbf{B}_r/\mu_0$ is the magnetic moment of the magnet, V is the magnet volume, μ_0 is the vacuum magnetic permeability, and $\mathbf{B}_r$ is the magnetic remanence. The magnetic torque tends to align the magnetic moment of the magnet with the magnetic field. For small magnets ($\leqslant$1mm) and a strong enough magnetic field ($\geqslant$10mT), the realignment dynamics can be neglected (see Supporting Information for the validation of this assumption) and we can assume $\mathbf{m} \| \mathbf{B}$.[30] In that case, the magnetic force expression can be simplified to

$$\mathbf{F}_{mag} = |\mathbf{m}|(\hat{\mathbf{B}} \cdot \nabla)\mathbf{B} \tag{2}$$

where $\hat{\mathbf{B}} = \mathbf{B}/|\mathbf{B}|$ is the unit vector in the direction of the field. To evaluate the currents that would result in a desired field and force at the magnet's position, the system's empirical model is solved numerically.[30] Refer to the Supporting Information for the mathematical derivation.

The support bath, being a yield-stress material, presents a complex relationship between the shear stress (τ) and shear strain ($\dot{\gamma}$). The rheology of a yield-stress material can be modeled as a Herschel–Bulkley fluid:

$$\begin{cases} \dot{\gamma} = 0 & \text{if } \tau < \tau_y \\ \tau = \tau_y + \nu_0 \dot{\gamma}_0 \left(\frac{\dot{\gamma}}{\dot{\gamma}_0}\right)^n & \text{if } \tau \geq \tau_y \end{cases} \tag{3}$$

where τ_y is the yield stress, ν_0 is the reference viscosity, $\dot{\gamma}_0$ is the reference shear rate, and n is the power-law coefficient. For $\tau < \tau_y$, the support bath behaves like a solid (unyielded state), and for $\tau \geqslant \tau_y$, the support bath behaves like a fluid (yielded state). In particular, for $n < 1$, the support bath behaves like a shear-thinning fluid in the yielded state. Finite-element simulations show that the movement of the magnet locally yields (fluidizes) the support bath while the rest of the bath remains unyielded, as shown in **Figure 2A**. Although at higher flow rates the yielded area can take complex shapes,[39,40] at the employed velocities (<3mms^{-1}), this area is quasi-spherical. The size of the yielded volume increases with the velocity of the magnet, as shown in Figure 2B. For details on the finite-element model, see Supporting Information.

Next, we model the dynamics of the magnet as a function of the applied magnetic force and the bath response. Since at micro/milli scales, the inertia of the magnet can normally be neglected,[31,33] we assume the magnet to instantaneously attain its terminal velocity upon applying a magnetic force (see Supporting Information for the validation of this assumption). Therefore, we propose to model the velocity of the magnet ($\dot{\mathbf{X}}$) in the support

© 2024 The Author(s). Advanced Materials Technologies published by Wiley-VCH GmbH

2365709x, 0, Downloaded from https://onlinelibrary.wiley.com/doi/10.1002/admt.202401097 by Universiteitsbibliotheek, Wiley Online Library on [11/10/2024]. See the Terms and Conditions (https://onlinelibrary.wiley.com/terms-and-conditions) on Wiley Online Library for rules of use; OA articles are governed by the applicable Creative Commons License

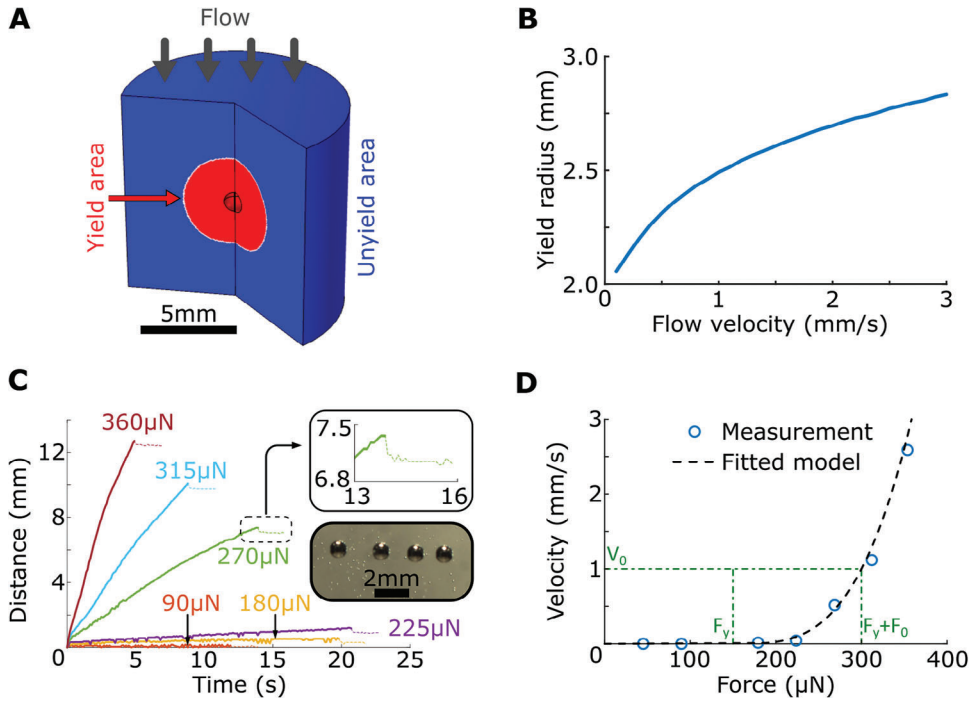

Figure 2. Magnet steering in a yield-stress bath. A) Finite element simulation of a yield-stress flow around a 1mm diameter sphere moving at 1mm/s. The flow presents a yielded (fluid) area close to the sphere and an unyielded (solid) area further away. B) Yield radius as a function of the flow velocity around a 1 mm sphere obtained through finite elements simulations. For details on the numerical model, see Supporting Information. C) Position evolution of a 1 mm spherical magnet in a 0.4% (w/v) Carbopol bath under different applied magnetic forces. Upon removal of the applied force, the magnet retracts for ≈0.3mm due to the viscoelastic nature of the media, as shown by the dashed lines. The inset shows a timelapse (4s intervals) of the movement of the magnet under a 270 μN magnetic force. D) Average velocity as a function of the applied magnetic force. The non-Newtonian behavior of the media results in a non-linear relationship between the applied force and the resulting velocity. The dashed line represents a fitted model with a yield force $F_y = 150\mu N$, a power law coefficient $n = 0.3$, and a reference drag force $F_0 = 150\mu N$ ($@\dot{x} = 1mms^{-1}$).

bath as a function of the applied force ($\mathbf{F}$). Adapting the fluid local behavior described by Equation (3) to macroscopic variables, we obtain:

$$\begin{cases} \dot{\mathbf{X}} = 0 & \text{if } |\mathbf{F}| < F_y \\ \mathbf{F} = \left(F_y + F_0\left(\frac{|\dot{\mathbf{X}}|}{\dot{X}_0}\right)^{n_F}\right)\hat{\dot{\mathbf{X}}} & \text{if } |\mathbf{F}| \geq F_y \end{cases} \tag{4}$$

where F_y is the yield force, F_0 is the reference force, $\dot{X}_0$ is the reference velocity, n_F is the power-law coefficient, and $\hat{\dot{\mathbf{X}}} = \dot{\mathbf{X}}/|\dot{\mathbf{X}}|$ is the velocity direction. In our case, the movement of a 1mm diameter spherical magnet (magnetic moment $\mathbf{m} = 5.8 \times 10^{-4} Am^2$) in a 0.4% (w/v) Carbopol support bath is characterized as a function of the applied magnetic force. Under a constant applied force, the magnet moves at an approximately constant velocity, as shown in Figure 2C. Interestingly, upon the removal of the applied force, the magnet moves back as a result of the relaxation of the elastic forces in the support bath. The average velocity of the magnet as a function of the applied force is shown in Figure 2D. These experimental values can be explained by Equation (4) with $n_F = 0.3$, $F_y = 150\mu N$, and $F_0 = 150\mu N$ for $\dot{X}_0 = 1mms^{-1}$. Although this complex dynamic behavior might hinder the precise positioning of the magnet using traditional control strategies, the steering of the magnet at an approximately constant velocity can be achieved by imposing a constant magnetic force magnitude.

2.3. Printing Water

To validate the MagNoFE3D technique, we print water in a 0.4%(w/v) Carbopol support bath. The injected water is colored pink with an acrylic emulsion for improved visualization. The first experiment consists of pulling the magnet (at $\approx 0.5mm\ s^{-1}$) from an inlet to an outlet while simultaneously injecting colored water (at $Q = 5\mu Lmin^{-1}$ flow rate), as shown in **Figure 3A**. Once the magnet reaches the outlet, it leaves behind a perfusable path from inlet to outlet. To facilitate the perfusion, the outlet tube is prefilled with colored water to prevent the high surface tension of the air-water interface from closing back the opened space once the magnet escapes. Notice that the printed channel width is larger near the inlet, and it also increases with time after printing. This can be attributed to water diffusing into the Carbopol bath, which can modify its properties.

As a second experiment, a 3D helical path is created by dynamically changing the direction of the applied magnetic force, as shown in Figure 3B. The prescribed path is followed with an average precision of 0.5mm. This precision could be further enhanced by implementing advanced closed-loop control techniques, such as Model Predictive Control, which could predict and optimize future movements, or Reinforcement Learning algorithms, which can learn and correct the system's deviations from the model. This demonstrates the capability of MagNoFE3D for the 3D embedded printing of aqueous inks in a granular

© 2024 The Author(s). Advanced Materials Technologies published by Wiley-VCH GmbH

2365709x, 0, Downloaded from https://onlinelibrary.wiley.com/doi/10.1002/admt.202401097 by Universiteitsbibliotheek, Wiley Online Library on [11/10/2024]. See the Terms and Conditions (https://onlinelibrary.wiley.com/terms-and-conditions) on Wiley Online Library for rules of use; OA articles are governed by the applicable Creative Commons License

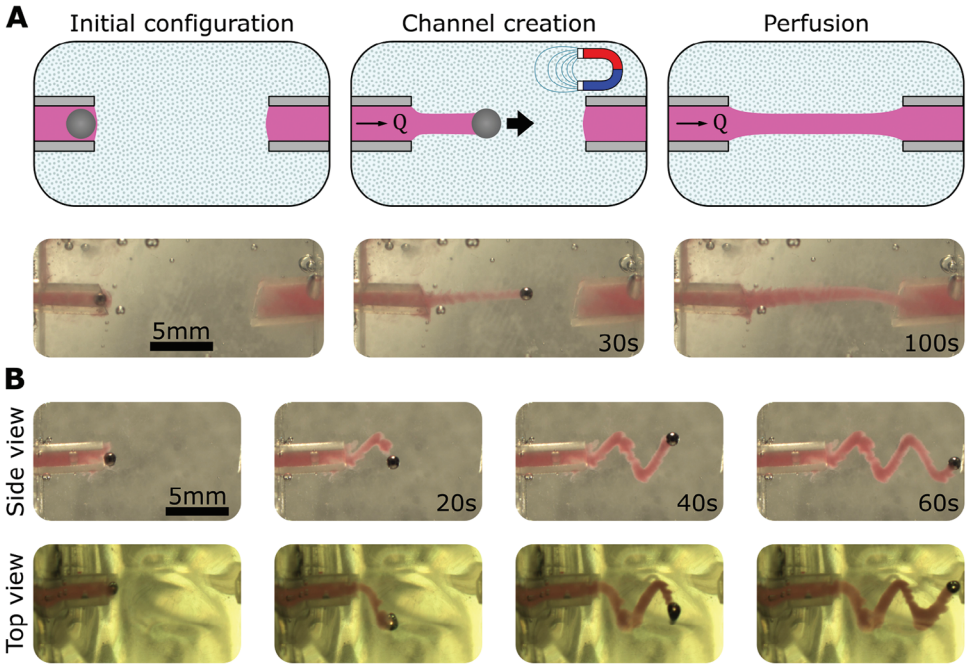

Figure 3. MagNoFE3D printing of water in a Carbopol support bath. A) Printing of a water (viscosity ν = 1mPas) straight line with an injection flow (Q = 5µL/min). The magnet reaches an outlet tube prefilled with colored water, achieving perfusion between the inlet and the outlet. See Video S1 (Supporting Information). B) Printing of a 3D double helix. The top view is distorted by optical refraction on the wavy surface of the support bath. See Video S2 (Supporting Information). The magnet velocity is ≈0.5mm s^{-1}.

support bath. As an additional validation, water is also printed in a Xanthan gum support bath using our MagNoFE3D technique, as shown in the Supporting Information. The use of this biocompatible support bath paves the way for bioprinting and cell culture applications.

2.4. Printing UV Resin

Another capability of the proposed MagNoFE3D technique is the printing of photocurable resins. In particular, by curing the resin with the magnet still present in the bath, we obtain a magnetically responsive structure. The process consists of first creating the channel by steering the magnet and using a UV resin as ink. Then, the created structure is cured using a UV lamp and exploiting the optical transparency of the Carbopol support bath. As a result, the solid cured structure, which incorporates the magnet, is responsive to externally applied fields. As a first example, we create a 7mm long straight horizontal beam with the magnet's magnetic moment pointing upwards, as shown in **Figure** 4A. Upon the application of an external field ($|\mathbf{B}|$ = 50mT) in either direction, the beam exhibits a total deflection of 50°. The diameter of the beam, measured to 770 ± 50 µm by image analysis, is mostly constant along the beam length. In this case, the photocurable resin does not diffuse into the Carbopol bath, which facilitates the stability of the printed structure. However, the cross-section of the printed structure can decrease with the distance from the inlet since the high viscosity (ν = 2500mPas) of the resin can lead to noticeable pressure drops during the printing process.

Furthermore, to showcase the 3D capability of the MagNoFE3D system, we show the creation of a 3D resin structure composed of segments along the three main axes. This is achieved by sequentially switching the advancing direction of the magnet during fabrication. Upon the application of an external field, the structure shows deformation of the different segments depending on the direction of the magnetic torque. Another capability of the MagNoFE3D system is the sequential printing of multiple photocurable structures. The process consists of printing and curing each structure sequentially. Since during the printing process, the magnetic field does not exceed 10mT, the deformations of the cured structures are negligible. As an example, a first pink straight line is printed and cured, and then, a blue straight line is printed, as shown in **Figure** 5. This approach opens the way for the creation of complex and multimaterial printing structures using the proposed MagNoFE3D technique.

3. Conclusion

In this work, we present a novel Magnetic Nozzle-Free Embedded 3D (MagNoFE3D) printing technique that utilizes a magnetic sphere as the plotting mechanism in embedded 3D printing. The proposed method consists of steering a magnetic sphere in a yield-stress support bath utilizing an external electromagnetic actuation system while simultaneously injecting the printing ink into the workspace. The movement of the magnet locally fluidized the support bath, opening space for the ink. By steering the magnet, we can guide the ink for the generation of 3D structures. The main advantage of our MagNoFE3D approach is that it localizes the disturbance to the support bath to the printing area around the sphere, in contrast to nozzle-based systems where the bath is perturbed along the entire length of

© 2024 The Author(s). Advanced Materials Technologies published by Wiley-VCH GmbH

2365709x, 0, Downloaded from https://onlinelibrary.wiley.com/doi/10.1002/admt.202401097 by Universitätsbibliothek, Wiley Online Library on [11/10/2024]. See the Terms and Conditions (https://onlinelibrary.wiley.com/terms-and-conditions) on Wiley Online Library for rules of use; OA articles are governed by the applicable Creative Commons License

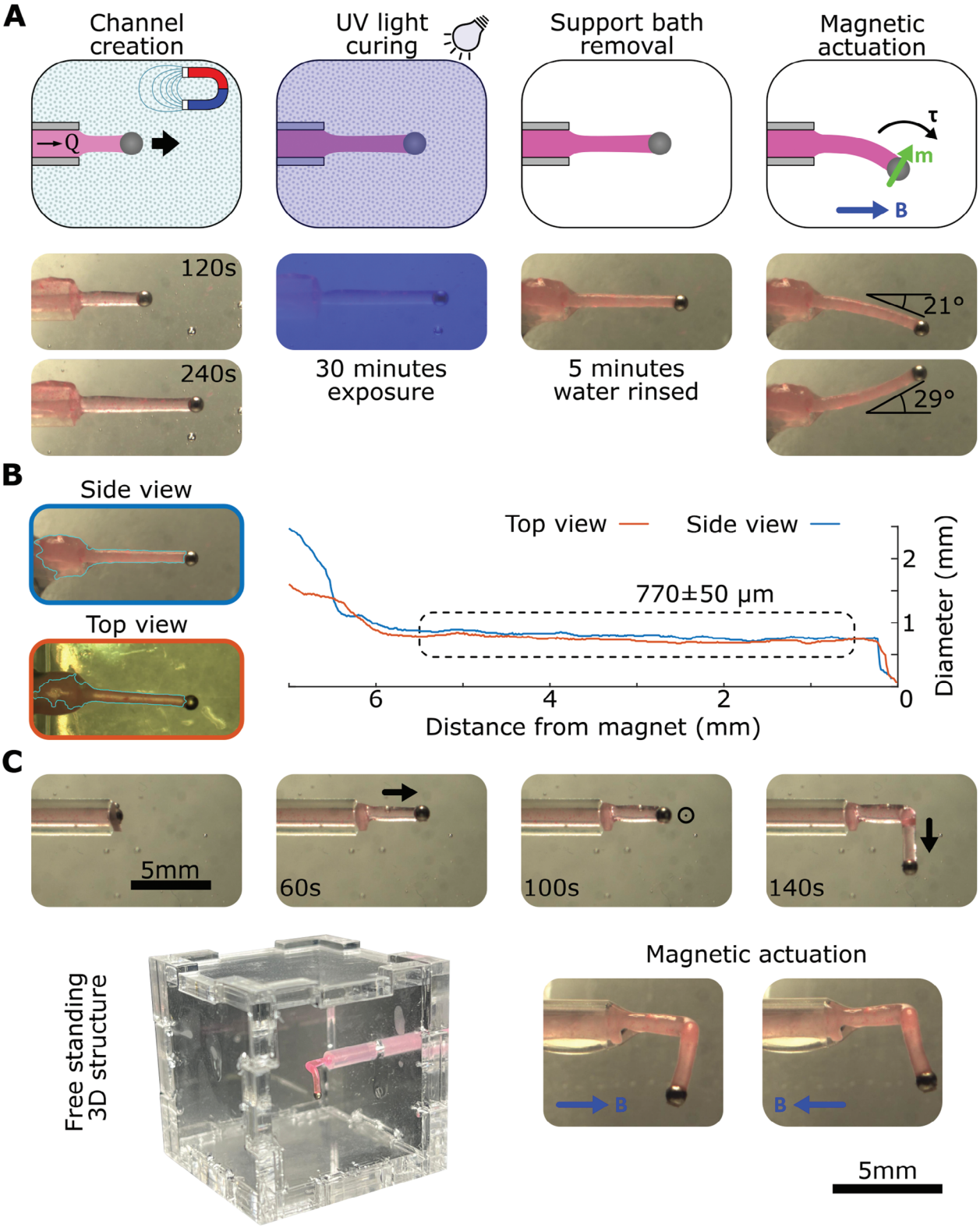

Figure 4. MagNoFE3D printing and curing of UV resin in a Carbopol support bath. A) Printing, curing, and actuation of a UV resin (Nordland Optical Adhesive 63, viscosity $\nu = 2500 mPa.s$) straight line. The actuating magnetic field ($|\mathbf{B}| = 50$mT) interacts with the magnetic moment of the magnet ($\mathbf{m} = 5.8 \times 10^{-4}$Am^2) generating a torque ($|\mathbf{T}_{mag}| = 29$µNm). See Video S3 (Supporting Information). B) The diameter of the printed beam is measured to be 770±50 µm and mostly constant along the beam length. C) Printing and actuation of a 3D structure. See Video S4 (Supporting Information).

© 2024 The Author(s). Advanced Materials Technologies published by Wiley-VCH GmbH

2365709x, 0, Downloaded from https://onlinelibrary.wiley.com/doi/10.1002/admt.202401097 by Universiteitsbibliotheek, Wiley Online Library on [11/10/2024]. See the Terms and Conditions (https://onlinelibrary.wiley.com/terms-and-conditions) on Wiley Online Library for rules of use; OA articles are governed by the applicable Creative Commons License

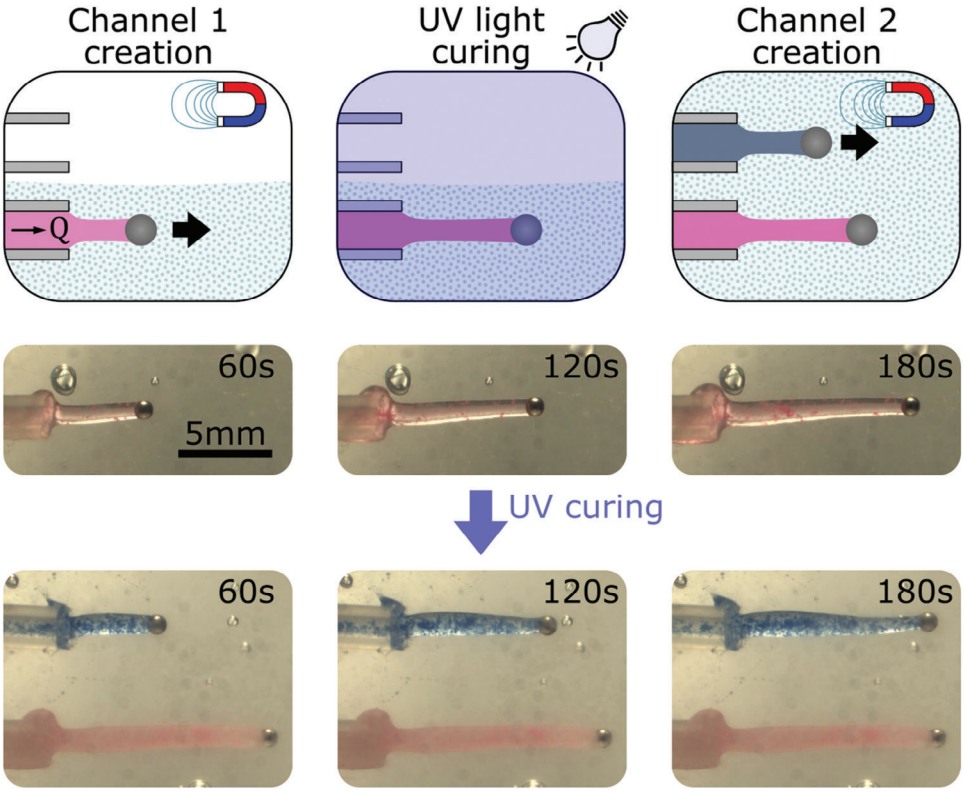

Figure 5. Sequential printing of photocurable structures. Printing of two straight lines in a 0.4% (w/v) Carbopol solution. The process consists of printing the first structure, curing it, and then printing the second structure. Since during the printing process the magnetic field never exceeds 10mT, the deformation of the cured structure is negligible. See Video S5 (Supporting Information).

the moving nozzle. This innovative approach enables the successful printing of low-viscosity inks, including water (viscosity 1mPa s), in three dimensions, and the printing of solid structures utilizing photocurable inks (viscosity ≈2500mPas), demonstrating a wide working range of ink viscosities and the compatibility with light-curing approaches due to the support bath transparency.

While the proposed system shows promising results, some possible future improvements have been identified. First, a possible improvement is to dynamically adjust the injection flow rate as a function of the measured magnet displacement to compensate for velocity variations. Alternatively, a pressure-controlled pump (as opposed to a volume-controlled pump) could regulate the pressure driving the ink into the cavity created by the moving magnet, ensuring consistent flow regardless of the magnet's velocity variations. Another possible improvement is the optimization of the geometry of the magnetic plotting agent. For example, helical microrobots have shown excellent capabilities to swim in non-Newtonian complex fluids.[41] Alternatively, remote heating of the magnetic agent[42] could enable the local liquefaction of the support bath, thus facilitating the printing. Finally, the properties of the support bath, both mechanical and chemical, can be adjusted for optimized printing. Microfludically produced hydrogel microparticle baths that are tunable both in size and composition would offer greater insight into the interplay between the ink and the bath, as well as enable a multitude of applications.[43] Looking forward, fine-tuning the interfacial properties between the bath and the ink could further stabilize the printing process. Moreover, recently developed programable metafluids[44] could allow for the adjustment of the support bath properties during the printing.

In conclusion, the proposed MagNoFE3D methodology demonstrates promising results and has the potential to advance embedded printing significantly. MagNoFE3D offers freedom and precision through magnetic 3D manipulation, enables the printing of low-viscosity inks, and improves resin efficiency compared to SLA polymerization techniques. MagNoFE3D can enable innovation in soft robotics, by allowing the direct fabrication of elastic and magnetically responsive structures, and bioprinting since it is compatible with cell culture support baths, such as Xanthan gum (as shown in the Supporting Information). The potential applications of MagNoFE3D for microrobotics and bioprinting could be enhanced by improving its resolution. Since the feature size is determined by the size of the plotting magnet, increasing the printing resolution can be achieved by utilizing smaller magnets. Nonetheless, since magnetic forces scale with the volume of the magnet while viscous forces scale with its diameter, utilizing smaller magnets would require either a more powerful magnetic actuation system or a lower viscosity support bath. However, reducing the viscosity of the bath could compromise its ability to stabilize the printed structure, creating a trade-off between resolution and structural integrity.

© 2024 The Author(s). Advanced Materials Technologies published by Wiley-VCH GmbH

2365709x, 0, Downloaded from https://onlinelibrary.wiley.com/doi/10.1002/admt.202401097 by Universiteitsbibliotheek, Wiley Online Library on [11/10/2024]. See the Terms and Conditions (https://onlinelibrary.wiley.com/terms-and-conditions) on Wiley Online Library for rules of use; OA articles are governed by the applicable Creative Commons License

4. Experimental Section

Electromagnetic System: The electromagnetic actuation system consists of nine Vacoflux-core coils placed 30mm from a common center, as shown in Figure 1. The system is capable of generating magnetic fields of up to 100mT and gradients of up to 1T m^{-1}. The coils are powered by Elmo Motion Control (Petach–Tikva, Israel) servo drives. The workspace, a 22 × 22 × 22mm Polymethyl methacrylate cubic box, is imaged by two Grasshopper 3 (FLIR, USA) cameras, from the side and the top, running at a frame rate of 10Hz. A desktop computer connected to the cameras and coil drivers runs the control algorithm implemented in a custom C++17 code on a Qt Creator 5.9 development environment. The control algorithm encompasses the communication with the cameras and coil drivers, code generated by MATLAB 2022b to numerically invert the dynamic model, and image analysis routines utilizing the Hough Transformation from OpenCV 4.6. The utilized magnet is a nickel-plated N50 neodymium spherical magnet (remanence $|\mathbf{B}_r| = 1.4$T) of 1mm diameter (HKCM Engineering, Germany). The magnetic moment of the magnet is $|\mathbf{m}| = 5.8 \times 10^{-4}\text{Am}^2$, allowing for a maximum theoretical torque of $\mathbf{T}_{mag} = 58\mu\text{Nm}$ and force of $\mathbf{F}_{mag} = 580\mu\text{N}$.

Fluidic System: The Carbopol support bath was prepared by weighting and dispersing Carbopol ETD2020 powder (Lubrizol, USA) in 1L of ultrapure Milli-Q water with a target concentration of 0.4% (w/v), under constant stirring for at least 4 h to allow dispersion and hydration of the carbomer. The pH of the solution is tuned to 7.4, using 0.1M hydrogen chloride (HCl), while monitoring with a pH meter. The gel suspension was subsequently centrifuged in a Beckman Avanti J–E centrifuge (Beckman Coulter Life Sciences, USA) at 770RCF to remove gas bubbles. Then, the Carbopol gel was poured, using a spatula for assistance, into the cubic recipient. The Xanthan gum support bath (see Supporting Information) was prepared by weighing and dispersing Xanthan gum powder (Xanthomonas Campestris, G1253, Sigma Aldrich, USA) in 1L of ultrapure Milli-Q water with a target concentration of 1.5% (w/v). The solution was constantly stirred overnight at room temperature to allow homogenous dispersion. The Xanthan gum gel was centrifuged at 770RCF to remove gas bubbles, and transported with a spatula to the cubic recipient.

To inject the ink, an ink-loaded 10mL (for water) or 5mL (UV resin) syringe was mounted on a NE-4000 Two Channel Programmable Syringe Pump (New Era Pump Systems, USA) and connected to the workspace through a silicone tube (Technirub, The Netherlands) of 1.2 and 2.5mm internal and external diameter, respectively. The water printing experiments were performed utilizing ultrapure Milli-Q water dyed with a pink acrylic emulsion (Acrylicos Vallejo S.L., Spain) for visualization (< 10%(v/v)). The UV resin printing experiments were performed utilizing Nordland Optical Adhesive 63 (Nordland Products, USA), with a room temperature viscosity of $\nu = 2500$mPas, also dyed in pink for visualization.

Supporting Information

Supporting Information is available from the Wiley Online Library or from the author.

Acknowledgements

F.N.P.B., V.D.T., J.R., and S.M. equally contributed to this work. This work was supported by the European Commission under the Horizon Europe program under Grant #101070066 (RĚGO). The authors want to thank Jakub Sikorski for his valuable feedback on the early conception of this work.

Conflict of Interest

The authors declare no conflict of interest.

Data Availability Statement

The data that support the findings of this study are available from the corresponding author upon reasonable request.

Keywords

3D printing, additive manufacturing, embedded printing, magnetic actuation, microrobotics

Received: July 8, 2024
Revised: September 25, 2024
Published online:

[1] Y. S. Zhang, G. Haghiashtiani, T. Hübscher, D. J. Kelly, J. M. Lee, M. Lutolf, M. C. McAlpine, W. Y. Yeong, M. Zenobi-Wong, J. Malda, *Nat. Rev. Methods Primers* **2021**, *1*, 75.
[2] S. You, Y. Xiang, H. H. Hwang, D. B. Berry, W. Kiratitanaporn, J. Guan, E. Yao, M. Tang, Z. Zhong, X. Ma, D. Wangpraseurt, Y. Sun, T. Lu, S. Chen, *Sci. Adv.* **2023**, *9*, eade7923.
[3] P. Zhang, I. M. Lei, G. Chen, J. Lin, X. Chen, J. Zhang, C. Cai, X. Liang, J. Liu, *Nat. Commun.* **2022**, *13*, 4775.
[4] J. Macedo, N. F. da Costa, V. Vanhoorne, C. Vervaet, J. F. Pinto, *J. Pharm. Sci.* **2022**, *111*, 2814.
[5] J. Mewis, N. J. Wagner, *Adv. Colloid Interface Sci.* **2009**, *147*, 214.
[6] I. T. Ozbolat, *3D Bioprinting: Fundamentals, Principles and Applications*, Academic Press, Cambridge, MA, usa **2016**.
[7] H. A. Barnes, *J. Non-Newtonian Fluid Mech.* **1997**, *70*, 1.
[8] A. Cano-Vicent, M. M. Tambuwala, S. S. Hassan, D. Barh, A. A. Aljabali, M. Birkett, A. Arjunan, Á. Serrano-Aroca, *Addit. Manuf.* **2021**, *47*, 102378.
[9] Z. Zheng, D. Eglin, M. Alini, G. R. Richards, L. Qin, Y. Lai, *Engineering* **2021**, *7*, 966.
[10] A. GhavamiNejad, N. Ashammakhi, X. Y. Wu, A. Khademhosseini, *Small* **2020**, *16*, 2002931.
[11] D. B. Kolesky, K. A. Homan, M. A. Skylar-Scott, J. A. Lewis, *Proc. Natl. Acad. Sci.* **2016**, *113*, 3179.
[12] P. Patpatiya, K. Chaudhary, A. Shastri, S. Sharma, *Proc. Inst. Mech. Eng., Part C: J. Mech. Eng. Sci.* **2022**, *236*, 7899.
[13] A. McCormack, C. B. Highley, N. R. Leslie, F. P. Melchels, *Trends Biotechnol.* **2020**, *38*, 584.
[14] T. Bhattacharjee, S. M. Zehnder, K. G. Rowe, S. Jain, R. M. Nixon, W. G. Sawyer, T. E. Angelini, *Sci. Adv.* **2015**, *1*, e1500655.
[15] S. G. Patrício, L. R. Sousa, T. R. Correia, V. M. Gaspar, L. S. Pires, J. L. Luís, J. M. Oliveira, J. F. Mano, *Biofabrication* **2020**, *12*, 035017.
[16] G. M. Gratson, M. Xu, J. A. Lewis, *Nature* **2004**, *428*, 386.
[17] T. J. Hinton, Q. Jallerat, R. N. Palchesko, J. H. Park, M. S. Grodzicki, H.-J. Shue, M. H. Ramadan, A. R. Hudson, A. W. Feinberg, *Sci. Adv.* **2015**, *1*, e1500758.
[18] T. Bhattacharjee, C. J. Gil, S. L. Marshall, J. M. Urueña, C. S. O'Bryan, M. Carstens, B. Keselowsky, G. D. Palmer, S. Ghivizzani, C. P. Gibbs, et al., *ACS Biomater. Sci. Eng.* **2016**, *2*, 1787.
[19] J. A. Brassard, M. Nikolaev, T. Hübscher, M. Hofer, M. P. Lutolf, *Nat. Mater.* **2021**, *20*, 22.
[20] V. D. Trikalitis, N. J. Kroese, M. Kaya, C. Cofiño-Fabres, S. Ten Den, I. S. M. Khalil, S. Misra, B. F. Koopman, R. Passier, V. Schwach, et al., *Biofabrication* **2022**, *15*, 015014.
[21] V. D. Trikalitis, J. Perea Paizal, V. Rangel, F. Stein, J. Rouwkema, *Tissue Eng., Part C* **2024**, *30*, 206.
[22] M. Wehner, R. L. Truby, D. J. Fitzgerald, B. Mosadegh, G. M. Whitesides, J. A. Lewis, R. J. Wood, *Nature* **2016**, *536*, 451.

© 2024 The Author(s). Advanced Materials Technologies published by Wiley-VCH GmbH

2365709x, 0, Downloaded from https://onlinelibrary.wiley.com/doi/10.1002/admt.202401097 by Universiteitsbibliotheek, Wiley Online Library on [11/10/2024]. See the Terms and Conditions (https://onlinelibrary.wiley.com/terms-and-conditions) on Wiley Online Library for rules of use; OA articles are governed by the applicable Creative Commons License

[23] B. Herren, M. C. Saha, M. C. Altan, Y. Liu, *Composites, Part B* **2020**, *200*, 108224.
[24] D. J. Shiwarski, A. R. Hudson, J. W. Tashman, A. W. Feinberg, *APL Bioeng.* **2021**, *5*, 1.
[25] J. Eggers, *Rev. Mod. Phys.* **1997**, *69*, 865.
[26] J. H. Cho, E. Dressaire, *Phys. Rev. Appl.* **2024**, *22*, 034050.
[27] G. Luo, Y. Yu, Y. Yuan, X. Chen, Z. Liu, T. Kong, *Adv. Mater.* **2019**, *31*, 1904631.
[28] R. Karyappa, W. H. Goh, M. Hashimoto, *ACS Appl. Mater. Interfaces* **2022**, *14*, 41520.
[29] J. J. Abbott, E. Diller, A. J. Petruska, *Annu. Rev. Control, Robot., Auton. Syst.* **2020**, *3*, 57.
[30] M. P. Kummer, J. J. Abbott, B. E. Kratochvil, R. Borer, A. Sengul, B. J. Nelson, *IEEE Tran. Robot.* **2010**, *26*, 1006.
[31] F. N. Piñan Basualdo, R. Van de Weerd, S. Misra, *IEEE Robot. Autom. Lett.* **2024**, *9*, 1788.
[32] M. Salehizadeh, E. Diller, *Int. J. Robotics Research* **2020**, *39*, 1377.
[33] F. N. Piñan Basualdo, S. Misra, *Adv. Intell. Syst.* **2023**, *5*, 2300365.
[34] B. J. Nelson, I. K. Kaliakatsos, J. J. Abbott, *Annu. Rev. Biomed. Eng.* **2010**, *12*, 55.
[35] M. Sitti, H. Ceylan, W. Hu, J. Giltinan, M. Turan, S. Yim, E. Diller, *Proc. IEEE* **2015**, *103*, 205.
[36] Y. Kim, X. Zhao, *Chem. Rev.* **2022**, *122*, 5317.
[37] Y. Deng, Y. Zhao, J. Zhang, T. Arai, Q. Huang, X. Liu, *Adv. Intell. Syst.* **2024**, *6*, 2300471.
[38] C. Zhang, X. Li, L. Jiang, D. Tang, H. Xu, P. Zhao, J. Fu, Q. Zhou, Y. Chen, *Adv. Funct. Mater.* **2021**, *31*, 2102777.
[39] D. Fraggedakis, Y. Dimakopoulos, J. Tsamopoulos, *Soft Matter* **2016**, *12*, 5378.
[40] M. Sarabian, M. E. Rosti, L. Brandt, S. Hormozi, *J. Fluid Mech.* **2020**, *896*, A17.
[41] S. Palagi, D. Walker, T. Qiu, P. Fischer, in *Microbiorobotics*, Elsevier, Amsterdam, Netherlands **2017**, pp. 133–162.
[42] A. Ramos-Sebastian, S.-J. Gwak, S. H. Kim, *Adv. Sci.* **2022**, *9*, 2103863.
[43] T. Kamperman, V. D. Trikalitis, M. Karperien, C. W. Visser, J. Leijten, *ACS Appl. Mater. Interfaces* **2018**, *10*, 23433.
[44] A. Djellouli, B. Van Raemdonck, Y. Wang, Y. Yang, A. Caillaud, D. Weitz, S. Rubinstein, B. Gorissen, K. Bertoldi, *Nature* **2024**, *628*, 545.

© 2024 The Author(s). Advanced Materials Technologies published by Wiley-VCH GmbH

2365709x, 0, Downloaded from https://onlinelibrary.wiley.com/doi/10.1002/admt.202401097 by Universiteitsbibliotheek, Wiley Online Library on [11/10/2024]. See the Terms and Conditions (https://onlinelibrary.wiley.com/terms-and-conditions) on Wiley Online Library for rules of use; OA articles are governed by the applicable Creative Commons License